

Anti-Arthritic Potential of Topically Delivered Rutin from Cationic Phytosomal Gel in FCA-Induced Arthritic Rat Model: *In Vitro* and *In Vivo* Investigation

Sentu Das ¹ , Malay K Das ^{1,*} , Sanjoy Das ¹ , L. Ronibala Singha ¹ , Punamjyoti Das ¹ 

¹ Drug Delivery Research Laboratory, Department of Pharmaceutical Sciences, Dibrugarh University, Dibrugarh, Assam 786004, India

* Correspondence: mkdps@dibru.ac.in;

Received: 25.07.2024; Accepted: 6.10.2024; Published: 25.11.2025

Abstract: The therapeutic application of conventional anti-arthritic drugs is greatly limited due to poor skin permeability, resulting in poor transdermal bioavailability. Cationic nanocarrier-based drug delivery systems enhance the penetration of anti-arthritic drugs into deeper skin layers by interacting with the negative charge of the skin membrane. Herein, we developed rutin-loaded cationic phytosomes (RTCPs) via thin-layer hydration and incorporated them into a 2% Carbopol 940 gel for convenient topical application. The formulation F3 was selected as the optimized RTCPs with an average size (527.6 nm), narrow polydispersity index (0.348), positive zeta potential (+25.5 mV), and entrapment efficiency of 80.82 ± 3.03 %. HR-TEM analysis ensured that the spherical morphology had a smooth surface. The polymeric hydrogel showed all the desirable characteristics essential for topical application. *Ex vivo* skin permeation studies showed that RTCPs-loaded polymeric hydrogel had a 6.47-fold higher permeability than free RT hydrogel. Furthermore, *in vivo* anti-arthritic evaluation, hematological, radiological, and histopathological studies showed better therapeutic efficacy of RTCP-loaded polymeric hydrogel in the FCA-induced arthritis rat model compared to the commercially available anti-arthritic gel. These findings suggest that well-developed RTCPs can enhance skin penetration and serve as a potential drug-delivery system for the long-term management of RA and other inflammatory diseases.

Keywords: rutin-loaded cationic phytosomes; rutin; rheumatoid arthritis; polymeric hydrogel; topical delivery.

© 2025 by the authors. This article is an open-access article distributed under the terms and conditions of the Creative Commons Attribution (CC BY) license (<https://creativecommons.org/licenses/by/4.0/>), which permits unrestricted use, distribution, and reproduction in any medium, provided the original work is properly cited. The authors retain copyright of their work, and no permission is required from the authors or the publisher to reuse or distribute this article, as long as proper attribution is given to the original source.

1. Introduction

Rheumatoid arthritis (RA) is a chronic, autoimmune, inflammatory disorder of the joints that affects approximately 0.5-1% of the world's adult population [1]. The clinical manifestations of this disease include synovial joint inflammation, autoantibody production, and irreversible destruction of bone and cartilage tissues, which lead to disability and the inability to participate in physical and social activities, increase mortality, and have a significant impact on the patient's quality of life [2,3]. Although the exact cause of RA is unknown, genetic and environmental factors have influenced its occurrence [4]. The main goal of treating RA is to reduce pain and inflammation[5]. Nonsteroidal anti-inflammatory drugs (NSAIDs) are a group of analgesic and anti-inflammatory agents that are mostly prescribed to

treat a broad range of acute and chronic painful inflammatory conditions. Acetylsalicylic acid was the first NSAID introduced into the market in 1899 under the name of aspirin [6]. NSAIDs are now commercially available in many countries in oral, parenteral, and topical dosage forms. In the UK, 20-24 million prescriptions for oral NSAIDs are dispensed annually, accounting for 5% of all National Health Service prescriptions [7]. Although oral NSAIDs are effective for symptomatic relief in arthritic conditions, their usefulness is often limited by dose-dependent adverse events (AEs), such as gastrointestinal disturbances, cardiovascular events, and renal toxicity [8, 9]. These risks could be higher in the case of RA because patients with RA frequently require higher doses of NSAIDs for a projected period [10]. Topical formulations could mitigate these risks by enabling site-specific, effective delivery of analgesic concentrations while minimizing systemic exposure [11]. In 2014, approximately 5.8 million NSAID prescriptions were dispensed in England, primarily for topical ibuprofen and diclofenac [12]. However, there are instances of reported adverse effects on the usage of topical NSAIDs, such as irritation, erythema, dry skin, and pruritus. Some patients also reported systemic side effects like headaches and gastrointestinal (GI) upset [13, 14].

There are ongoing efforts to develop safer, more effective therapeutic agents with fewer side effects for long-term RA treatment. Several researchers have concluded that plant-derived phytochemicals are safe and effective for RA management [15]. Rutin is a naturally occurring bioflavonoid with excellent therapeutic properties, including antioxidant, anti-inflammatory, neuroprotective, antiallergenic, antiviral, and anticarcinogenic effects. Among these beneficial effects, the anti-inflammatory activity of rutin has been well established in the literature, and its application in treating various inflammatory diseases, including RA, has been reported [16,17]. Rutin generally reduces the generation of pro-inflammatory cytokines in arthritis-induced rats while suppressing the activity of induced nitric oxide synthase and cyclooxygenase-2 [18,19]. Another study suggested that rutin inhibits the transcription of 20 genes encoding critical pro-inflammatory factors, including tumor necrosis factor- α (TNF- α), interleukin-1 (IL-1), interleukin-8 (IL-8), migration inhibitory factor (MIF), and chemotactic factors, in activated human macrophages. Further studies revealed that rutin inhibited the overproduction of oxygen radicals in RA patients in an efficient manner [20]. Despite the potent anti-inflammatory effects and high safety profile of rutin, its therapeutic application via the topical route is severely limited by poor skin permeability, resulting in low transdermal bioavailability [21].

Nanotechnology-based drug delivery systems are a fascinating area of pharmaceutical science that has gained popularity due to their wide range of promising applications across high-impact areas of pharmaceutical research. Among others, phytosomes have recently attracted significant attention in topical drug delivery systems due to their unique physicochemical properties, such as amphiphilicity, non-immunogenicity, biocompatibility, and non-toxicity [22]. Phytosomes are structurally similar to liposomes and are formed through the conjugation of phospholipids and phyto-active components [23]. Due to the amphiphilic nature of phytosomes, they can easily penetrate the deeper layers of the skin pores and enhance the therapeutic efficacy of formulations [24]. Phytosomes enhance drug penetration into the skin and slow the release of encapsulated drugs while minimizing systemic exposure [25]. Moreover, charged nanocarriers are promising drug carriers for percutaneous administration [26]. Cationic nanocarrier-based drug delivery systems promote the penetration of water-insoluble drugs into deeper layers of skin via interactions with the negative charge of the skin membrane. Additionally, cationic nanocarriers have greater physical stability and

encapsulation ability due to their surface charge [27]. Interestingly, no one has reported rutin-loaded cationic phytosomes (RTCPs).

In the present study, we developed a novel RTCPs. Meanwhile, the phospholipid (soy lecithin) is the main active ingredient that forms lipid-compatible complexes (phytosomes) that interact with the polar functional groups of the drug molecules through hydrogen bonding. Thus, improves drug solubility, encapsulation efficiency, and loading capacity. Stearylamine (SA) is a positively charged lipid. It imparts a cationic charge to the surface of phytosomes, thereby increasing the skin permeation and bioavailability of water-insoluble drug molecules such as rutin, as the surfaces of all tissues contain a higher ratio of negatively charged lipids [28]. RTCPs cause an intensive interaction with the negatively charged lipids of the stratum corneum, leading to enhanced drug penetration through the skin.

Further, RTCPs were incorporated into the polymeric hydrogel, as it is easy to administer, causes no pain during application, has no first-pass effects, and can be delivered directly to the affected area. To the best of our knowledge, this is the first report on RTCPs-loaded polymeric hydrogel, demonstrating that it improves penetration-enhancing ability compared to RTNCPs-loaded polymeric hydrogel. Furthermore, compares its *in vivo* anti-arthritic efficacy with that of the commercially marketed product to assess a relatively safe and effective treatment for RA.

2. Materials and Methods

2.1. Materials.

Rutin (RT), phosphatidylcholine (PC) (Soy lecithin), and stearylamine (SA) were procured from TCI Chemicals Pvt. Ltd., Mumbai, India. Carbopol 940, methanol, and chloroform were purchased from HiMedia Laboratories Pvt. Ltd., Mumbai, India. Freund's Complete Adjuvant (FCA) was bought from Sigma-Aldrich, Bengaluru, India. Apart from that, all chemicals and reagents used were of analytical grade.

2.2. Preparation of phytosomes.

Rutin-loaded cationic phytosomes (RTCPs) were prepared by a thin-layer hydration method with various molar ratios of RT to PC and SA (Table 1) [29]. Accurate weighted quantities of PC and SA were dissolved in chloroform, while RT was dissolved in methanol. The two solutions were mixed thoroughly and stored at 7°C for 12 hours. The mixture was then transferred to a round-bottom flask (RBF) and evaporated at 45°C in a rotary evaporator (RV 10, IKA, Germany) until all of the solvent had evaporated. Thereafter, phosphate buffer at pH 6.8 was added to hydrate the thin film that had formed on the walls of the round flask, resulting in colloidal dispersions. To obtain a homogenized colloidal dispersion, the colloidal dispersions were sonicated for 10 min using an ultrasonic bath (UCB 30, Spectra Lab Instruments, India). Finally, the developed formulations were freeze-dried (temperature of -78°C and pressure of 0.02 mbar) using a lyophilizer (SS1-LYO, Southern Scientific Lab Instruments, India) with 3 % mannitol as a cryoprotectant and then stored in an airtight container for further use. Similarly, RTNCPs were also prepared without SA (Table 1). Furthermore, all the developed formulations were dispersed in distilled water to investigate their vesicle formation via particle size determination (Figure S1)

Table 1. Composition of various phytosomes formulations.

Ingredients	F1 (1:1) ^a	F2 (1:2) ^b	F3 (1:2:0.5) ^c	F4 (1:2:0.75) ^d
Rutin (mg)	15	15	15	15
Soy lecithin (mg)	18.65	37.28	37.28	37.28
Stearylamine (mg)	-	-	3.32	4.96
Methanol (ml)	10	10	10	10
Chloroform (ml)	10	10	10	10

Where F1 (1:1)^a and F2 (1:2)^b formulations are rutin-loaded non-cationic phytosomes (RTNCPs), F3 (1:2:0.5)^c and F4 (1:2:0.75)^d formulations are rutin-loaded cationic phytosomes (RTCPs).

2.3. Physicochemical characterization of phytosomes.

2.3.1. Particle size (PS), polydispersity index (PDI), and zeta potential (ZP) analysis.

Freshly prepared freeze-dried phytosomes were dispersed in 0.1% w/v double-distilled water to determine PS, PDI, and ZP. A particle size analyzer was used to determine the PS and PDI of the prepared phytosomes (90 Plus, Brookhaven Instruments, USA). The ZP of prepared phytosomes was determined by Zetasizer (Nano ZS, Malvern Instruments, UK) [30].

2.3.2. Drug entrapment efficiency (DEE) and drug loading (DL).

An accurate weight of phytosomes was added to 25 mL of phosphate buffer, pH 6.8, in a 50 mL beaker. The contents were stirred for 6 hours, then allowed to stand for 1 hour. The clear liquid was decanted and centrifuged for 30 minutes at 11500 rpm (R 8C DX, REMI, India). The supernatant was filtered through a 0.45 μm Whatman filter paper, and after appropriate dilution with phosphate buffer, absorbance was measured at 266 nm using a UV-visible spectrophotometer (UV-1800, Shimadzu, Japan) [30]. The following equation was used to calculate the DEE and DL.

$$DEE\% = \frac{\text{Actual drug content}}{\text{Theoretical drug content}} \times 100 \quad (1)$$

$$DL\% = \frac{\text{Actual drug content}}{\text{Yield of phytosomes formulation}} \times 100 \quad (2)$$

2.3.3. Drug-excipient compatibility studies.

FT-IR and DSC analyses were performed on the drug, lipid, physical mixture, optimized RTCPs (F3), and RTNCPs (F2) to assess possible interactions among the drug, lipid, and formulations [31].

The FT-IR of RT, PC, SA, physical mixture, RTCPs (F3), and RTNCPs (F2) was performed in the mid-IR region (wave number 500-4000 cm⁻¹) using an FT-IR spectrometer (Alpha, Bruker, Germany).

The DSC of RT, PC, SA, physical mixture, RTCPs (F3), and RTNCPs (F2) was performed using a Perkin Elmer DSC 4000 with an N₂ purge gas flow rate of 20 ml min⁻¹ and a heat flow rate of 10°C min⁻¹.

2.3.4. High-resolution transmission electron microscopy (HR-TEM).

HR-TEM (JEM-2100, JEOL, Japan) was used to investigate the morphology of phytosomes. The prepared phytosomes were dispersed in distilled water, and one drop of solution was placed on a carbon-coated copper grid. Before loading the grid surface into the specimen holder, it was thoroughly air-dried. After that, samples were examined under the microscope, and images were taken [32].

2.3.5. Saturated solubility studies.

The saturated solubility studies were performed by taking an excess sample and adding it to 5 ml of phosphate buffer, pH 6.8. The mixture was shaken vigorously for 48 hours at $37\pm 0.5^\circ\text{C}$ in a water bath. The sample was then filtered, suitably diluted, and analyzed using a UV-visible spectrophotometer at 266 nm [33].

2.3.6. *In vitro* drug release studies.

An *in vitro* drug release study was carried out using the dialysis bag method to determine the cumulative amount of RT release from the phytosomes formulations [34]. Initially, the dialysis membrane (molecular weight 12000 Da) was soaked in distilled water and subsequently filled with 2 ml of phytosomes dispersion (equivalent to 2 mg of free RT). The dialysis membrane was immersed in a 200 ml beaker containing 100 ml of dissolution medium (Phosphate buffer, pH 6.8, +40 % v/v PEG 400). During the experiment, the dissolution medium temperature was kept at $37\pm 0.5^\circ\text{C}$, and the rotation speed was set to 150 rpm. At predetermined intervals, 3 mL of liquor was withdrawn from the sampling pot and replaced with an equal volume of fresh buffer to maintain the sink condition. The cumulative amount of RT released from the phytosomes formulations was quantified using a UV-visible spectrophotometer at 266 nm after suitable dilution with phosphate buffer, pH 6.8. Furthermore, *in vitro* release data for phytosomes formulations were evaluated using various kinetic models, including zero-order, first-order, Higuchi, and Korsmeyer-Peppas models.

2.3.7. Stability studies.

The stability studies of all developed formulations were carried out by ICH guidelines [35]. In brief, all developed phytosomes formulations were stored in airtight containers for 3 months under two conditions: normal ($25\pm 2^\circ\text{C}$ and 75±5% RH) and refrigerated ($4\pm 2^\circ\text{C}$ and 75±5% RH) (Table S1). Samples were withdrawn at regular intervals (0, 30, 60, and 90 days) and examined for particle size, polydispersity index, drug entrapment efficiency, and drug loading.

2.4. Preparation of polymeric hydrogel.

Carbopol 940 was employed as a gelling agent for the formulation of polymeric hydrogel [36]. Briefly, Carbopol 940 was dispersed in a small volume of distilled water and stored overnight to ensure complete hydration. The hydrogel was then thoroughly mixed into the optimized RTCPs (F3) formulation and continuously stirred at 450 rpm for 20 minutes. Subsequently, methylparaben and glycerine were added to the prepared hydrogel, serving as preservatives and humectants, respectively. Finally, the hydrogel pH was adjusted to skin pH by incorporating triethanolamine solution dropwise.

Table 2. Composition of various polymeric hydrogel formulations.

Gel formulation	Carbopol 940 (% w/v)	Free RT	Phytosomes formulation (mg)	Glycerin (% w/v)	Methyl paraben (% w/v)	Triethanolamine	Distilled water
MGH1	2	10	-	4	0.6	q.s	q.s
MGH2	2	-	515.45 (F2)	4	0.6	q.s	q.s
MGH3	2	-	476.15 (F3)	4	0.6	q.s	q.s

Where MGH2 and MGH3 are equivalent to 10 mg of free RT, MGH1- Hydrogel containing free RT, MGH2- Hydrogel containing RTNCPs, and MGH3- Hydrogel containing RTCPs.

The hydrogel was then allowed to stand overnight to allow the trapped air to escape. Similarly, RTNCPs and free RT-loaded polymeric hydrogel were developed. The composition of all developed polymeric hydrogel formulations is shown in Table 2.

2.5. Characterization of polymeric hydrogel.

2.5.1. Physical appearance.

The physical appearance of the hydrogel was visually examined for color, homogeneity, and texture, while greasiness was assessed by applying it to the skin surface [37].

2.5.2. pH measurement.

pH of hydrogel was measured using a digital pH meter (pHTestr 10, Eutech Instruments, Singapore). Dip the pH meter electrode into the hydrogel dispersion and record the reading [37].

2.5.3. Consistency measurement.

The consistency of the prepared hydrogel was determined by dropping a cone attached to a holding rod from a fixed distance of 10 cm and allowing it to fall into the center of a glass cup filled with hydrogel. The cone penetration was accurately measured from the hydrogel surface to the inside. The distance traveled by the cone after 10 s was noted [38].

2.5.4. Gels strength.

To determine the strength of the prepared hydrogel, 50 g of hydrogel was placed in a 100 ml measuring cylinder, which was then placed in a thermostatically controlled water bath at 37°C. A calibrated weight of 35 g was slowly placed on the surface of the gel. The time (in seconds) required by the weight to penetrate 5 cm deep into the hydrogel was recorded [39].

2.5.5. Viscosity measurement.

The viscosity of the hydrogel was determined using a Brookfield viscometer (S-62, model LVDV-E) at 25°C with the viscometer rotated at 12 rpm [40].

2.5.6. Spreadability measurement.

The hydrogel spreadability was determined using the parallel-plate method [41]. 2 g of prepared hydrogel was placed between two glass plates (20×20 cm²). To spread the hydrogel, a weight of 500 g was placed on a glass plate for 5 minutes. The time required to separate the upper glass plate from the lower glass plate was considered a measure of spreadability. The following formula calculated the spreadability:

$$S = \frac{M.L}{T} \quad (3)$$

Where S-Spreadability; M-Upper glass plate mass; L- Glass plate length; T-Time required to separate.

2.5.7. Drug content determination.

To determine the drug content of the formulated hydrogel, about 1 g of the prepared hydrogel was dispersed in 20 mL of methanol. The mixture was shaken for two hours to ensure that the drug was completely dissolved. The solution was then filtered through a Whatman syringe filter, and the drug content was determined using a UV-visible spectrophotometer at 257nm [42].

2.5.8. *Ex vivo* skin permeation studies.

Ex vivo skin permeation studies of developed polymeric hydrogel formulations were carried out on excised rat abdominal skin. The healthy Wister albino rats weighing 150-200 g were sacrificed by inhaling excessive amounts of chloroform. Their hair was removed using an electric trimmer (NHT 1065, NOVA, India), and abdominal skin (5×5 cm²) was carefully excised. The surface-adhered debris and fats were carefully scraped and removed with forceps. The skin sample was then thoroughly cleaned with distilled water, blotted dry, and visually inspected for defects. Finally, the processed skin samples were stored at -20°C containing 1% formalin solution.

The permeation experiment was performed in a vertically modified Franz-type diffusion cell with a permeation area of 1.77 cm². In brief, a pre-treated skin sample was carefully introduced between the donor and receptor chambers of the Franz diffusion cell, with the dermis facing toward the receptor chamber. The donor chamber was filled with 1 g of prepared hydrogel (equivalent to 2 mg of free RT) and covered with aluminum foil to prevent drying out and contamination. The donor chamber was then carefully inserted into the receptor chamber while the dermis remained in close contact with the receptor solution (phosphate buffer, pH 6.8 + 40% v/v PEG 400), and the solution temperature was maintained at 37±0.5°C using a recirculating water bath. The entire assembly was mounted on a magnetic stirrer (RCT-B-S022, IKA, India) with stirring set to 250 rpm. The experiment was run for 24 hours. At specific time intervals, 3 ml of liquor were withdrawn from the sampling port and replaced with an equivalent volume of fresh buffer to maintain the sink condition. The collected samples were then analyzed using a UV-visible spectrophotometer at 266 nm against the blank buffer.

The permeation profiles were established by plotting the cumulative amount of drug permeated per unit area of skin (µg/cm²) vs. time (h). The steady-state permeation flux (*J_{ss}*, µg/cm²/h) of RT was calculated from the slope of the linear regression plot [43]. The apparent permeation coefficients (*P_{app}*, cm/h) were calculated using the following equation:

$$P_{app} = \frac{J_{ss}}{C_0} \quad (4)$$

Where *C₀* is the initial concentration RT (µg/ml) in the donor compartment.

2.5.9. Skin retention studies.

After the permeation experiment, the skin was removed from the diffusion cell, thoroughly washed with distilled water, and blotted dry. The dried skin was then chipped into small pieces and immersed in 10 ml of methanol for 24 hours. The skin pieces were then homogenized with the tissue homogenizer and centrifuged for 10 minutes to obtain the clear supernatant. The supernatant was collected and analyzed by UV-visible spectrophotometry at 257 nm [44].

2.5.10. *In vivo* anti-arthritic activities.

All animal experimental protocols were approved and conducted in accordance with the Institutional Animal Ethical Committee (IAEC) guidelines of the Department of Pharmaceutical Sciences, Dibrugarh University, Dibrugarh, Assam, India, under Approval No. IAEC/DU/202, Dated. 19/05/2021. Male Wister albino rats (6-8 weeks old) weighing approximately 150-200 g were randomly divided into five groups with four animals in each group. Group I was considered a normal control group (healthy rats), Group II was considered an arthritic control group (FCA-induced rats), Group III was considered a free RT hydrogel treated group (10 mg/kg), Group IV was considered as a RTCPs-loaded hydrogel treated group (equivalent to 10 mg of free RT) and Group V was considered as a standard group (marketed 1% diclofenac sodium gel). Arthritis was induced in Groups II to V by injecting FCA (0.1 ml) into the subplantar area of the left hind paw, and the animals were kept for 2 weeks to ensure complete arthritis development. The development of arthritis was confirmed by observing the normal rat paw and the degree of inflammation in the FCA-induced rat paw 24 hours after the injection (Figure 1). Thereafter, all rats were treated with free RT hydrogel, RTCP-loaded hydrogel, and marketed 1% diclofenac sodium gel once a day for 2 weeks. Disease severity was evaluated by measuring the changes in the rat's paw thickness and body weight from day 0 to 28 days [45].



Figure 1. Shows (a) a normal rat paw; (b) the degree of inflammation in an FCA-induced rat paw 24 hours after injection.

2.5.11. Hematological parameters.

On the last day of the experiment, all animals were anesthetized with chloroform, and blood samples were drawn by puncturing the retro-orbital plexus. Hematological parameters such as red blood cell (RBC) and white blood cell (WBC) were measured [46].

2.5.12. Radiological analysis.

Rutin is a polyphenolic flavonoid compound, so determining its anti-arthritic potential is very important [47]. The X-ray technique was used to investigate the development of arthritis in FCA-induced rats. This study aimed to compare the therapeutic effects of the treated groups with those of the control groups (normal and arthritic). Radiological analysis was performed on the last day of the experiment, prior to anesthetizing all animals with chloroform. Crucial precautions were taken throughout the experiment to reduce radiation exposure, including lead-impregnated aprons, gloves, thyroid shields, and eye shields.

2.5.13. Histopathological examination.

Histopathological examination was performed on full-thickness rat paw skin samples to investigate the anti-inflammatory response of the developed polymeric hydrogel <https://nanobioletters.com/>

formulations. The skin samples were collected from different animal groups. The skin samples were then thoroughly cleaned with phosphate buffer saline (PBS) and soaked in 10% formaldehyde solution for 18 hours. The collected skin samples were cut into 5 μ m sections and stained with hematoxylin and eosin. These skin samples were examined under a light microscope (BX 40, Olympus, Japan), and photographs were taken [48].

2.5.14. Statistical analysis.

All quantitative data were presented as mean \pm SD (n=3), and they were analyzed using Student's T-test analysis. A value of $p\leq 0.05$ and $p\leq 0.005$ was considered statistically significant.

3. Results and Discussion

3.1. Results.

3.1.1. Preparation of phytosomes.

The RTCPs were successfully prepared via thin-layer hydration at various molar ratios of RT to PC and SA. Methanol was chosen for dissolving RT, but PC and SA are insoluble in this mixture. PC and SA are soluble in chloroform. Methanol and chloroform are miscible with each other at any given volume. RT, PC, and SA were dissolved in methanol and chloroform, respectively. Then, the two solutions were well mixed and kept at 7 $^{\circ}$ C for 12 hours to form more stable hydrogen bonds. The obtained solution was then transferred to an RBF and evaporated in a rotary evaporator at a specific rpm and temperature until the solvent was completely evaporated. The thin layer formed on the RBF's wall was hydrated with phosphate buffer (pH 6.8) to form a colloidal dispersion. Similarly, RTNCPs were also developed without SA. All developed formulations appear to be vesicular in nature, with a pale yellow color in aqueous media.

3.1.2. Particle size, polydispersity index, and zeta potential analysis.

Table 3 shows the PS, PDI, and ZP of the developed RTCPs (F3, F4) and RTNCP (F1, F2). The average PS and PDI of both the RTCPs and RTNCP were measured by the Dynamic Light Scattering (DLS) technique using the particle size analyzer (90 Plus, Brookhaven Instrument, USA), and the ZP was measured by Zetasizer (Nano ZS, Malvern Instruments, UK) (Figure S2). The average PS of the RTCPs was found in the 527.6-548.4 nm range, with a PDI of 0.324-0.348 and ZP values of +25.5-+29.7 mV. On the other hand, the average PS of RTNCPs was found in the range of 335.6 to 429.5 nm, with a PDI of 0.324 to 0.348 and a ZP value of -21 to -24 mV. However, the average PS of optimized RTCPs (F3) was 527.6 nm, with a PDI of 0.348 and a ZP of +25.5 mV. These results indicate that different molar ratios of RT to PC and SA significantly affected PS, PDI, and ZP.

3.1.3. Drug entrapment efficiency and drug loading.

DEE and DL of both the RTCPs (F3, F4) and the RTNCPs (F1, F2) were evaluated using a UV-visible spectrophotometer (UV-1800, Shimadzu, Japan), and the results are presented in Table 3. These results showed that RTCPs have higher DEE and DE than RTNCPs. However, when the molar ratio of SA content exceeded 4.96 (F4), it significantly

decreased DEE ($76.68 \pm 2.00\%$) and DL ($2.05 \pm 0.16\%$). These findings suggest that optimal concentration of SA aids in DEE and DL.

Table 3. Characterization of various phytosomes formulations (n=3).

Formulation code	PS (nm)	PDI	ZP (mV)	DEE (%)	DL (%)
F1 (1:1)	429.5	0.269	-21	66.12 ± 2.57	1.91 ± 0.12
F2(1:2)	335.6	0.252	-24	69.49 ± 1.23	1.94 ± 0.23
F3(1:2:0.5)	527.6	0.348	+25.5	80.82 ± 3.03	2.10 ± 0.10
F4 (1:2:0.75)	548.4	0.324	+29.7	76.68 ± 2.00	2.05 ± 0.16

3.1.4. Drug-excipient compatibility studies.

Figure 2 shows the characteristics of the FT-IR spectra of pure drug RT, PC, SA, physical mixture, optimized RTCPs (F3), and RTNCPs (F2).

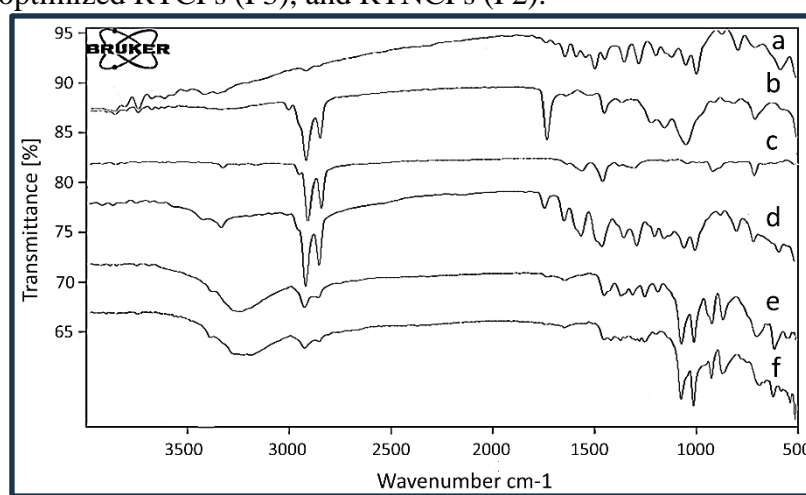


Figure 2. FT-IR spectrums of (a) pure drug RT; (b) PC; (c) SA; (d) physical mixture (RT: PC: SA); (e) RTNCPs (F2); (f) RTCPs (F3).

RT exhibited FT-IR peaks at 2922.95 cm^{-1} (C-H stretching), 597.27 cm^{-1} (C=C stretching), and 1651.31 cm^{-1} (aromatic ring). The PC showed two IR absorption peaks at 2854.48 and 2922.87 cm^{-1} due to the C-H stretching frequency of the long fatty acid chain, a C=O stretching peak at 1740.60 cm^{-1} in the fatty acid ester, a P=O stretching peak at 1163.54 cm^{-1} , a P-O-C stretching peak at 1057.89 cm^{-1} , and a $\text{N}^+(\text{CH}_3)_3$ stretching at 825.34 cm^{-1} . The FT-IR spectrum of SA exhibited two broad absorption peaks at 3331.39 cm^{-1} and 1569.04 cm^{-1} corresponding to N-H stretching and N-H bending vibrations, respectively. Strong absorption peaks were observed at $2800\text{-}3000 \text{ cm}^{-1}$ due to C-H stretching vibrations of SA. The C-N and C-H bending occur at 1467.21 cm^{-1} and 1051.71 cm^{-1} , respectively. The FT-IR spectra of the physical mixture of RT, PC, and SA exhibited all the characteristics of absorption bands of individual components without any notable variations. However, the intensity of the O-H peak in both the RTCPs and RTNCPs was reduced compared to the pure drug RT.

Figure 3 shows the DSC thermogram characteristics of pure drugs RT, PC, and SA, the physical mixture, and the optimized RTCPs (F3) and RTNCPs (F2). The DSC thermogram of RT showed two broad endothermic peaks at 154.26°C and 179.17°C , indicating the melting point of RT. At the same time, PC showed endothermic peaks at 116.48°C and 139.81°C , respectively. The SA showed a sharp endothermic peak at 61.59°C , which corresponds to its melting point. The physical mixture of RT, PC, and SA showed three endothermic peaks at 153.59°C , 106.88°C , and 54.91°C , respectively. The endothermic peak of PC was shifted from 116.48°C to 106.88°C , indicating a minor interaction took place between PC and RT. The DSC

thermogram of RTCPs exhibited three endothermic peaks at 56.20°C, 99.16°C, and 232.15°C, while RTNCPs showed two endothermic peaks at 145.18°C and 233.56°C, respectively. These results indicate that RT was completely embedded into the phospholipid matrix.

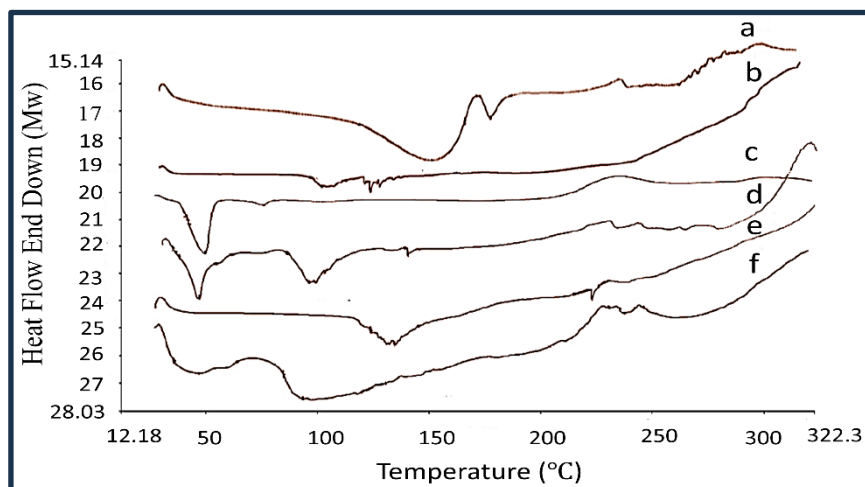


Figure 3. DSC thermograms of (a) pure drug RT; (b) PC; (c) SA; (d) physical mixture (RT: PC: SA); (e) RTNCPs (F2); (f) RTCPs (F3).

3.1.5. High-resolution transmission electron microscopy (HR-TEM).

The HR-TEM images of RTCPs (F3) and RTNCPs (F2) are shown in Figure 4. The images revealed the formation of distinct vesicle shapes without any aggregation or decomposition. The internal diameters of the RTCPs and RTNCPs were found in the 320.5 to 525 nm ranges. Furthermore, HR-TEM images show numerous small, dense, spherical bodies.

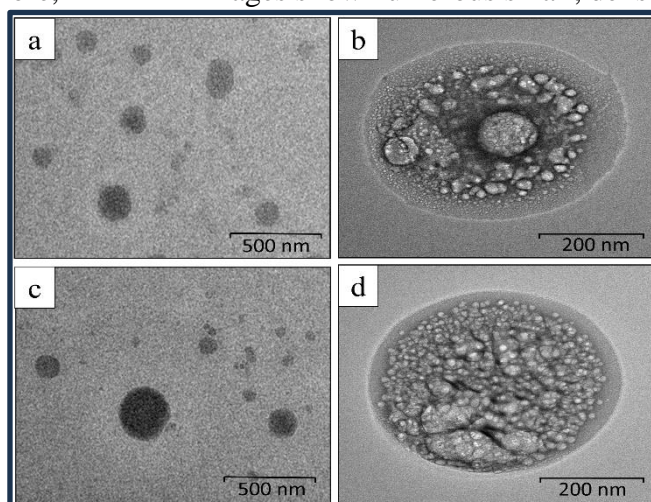


Figure 4. HR-TEM images of (a, b) RTNCPs (F2); (c, d) RTCPs (F3) at magnification of 5000X and 12000X, respectively.

3.1.6. Saturated solubility studies.

Rutin is a hydrophobic compound with low aqueous solubility, which limits its bioavailability and clinical utility. The obtained results (Figure 5) show that the free RT solubility in phosphate buffer pH 6.8 was 0.341 ± 0.042 mg/ml, while the F1, F2, F3, and F4 formulations were 0.724 ± 0.034 mg/ml, 0.780 ± 0.052 mg/ml, 0.716 ± 0.036 mg/ml, and 0.697 ± 0.042 mg/ml, respectively.

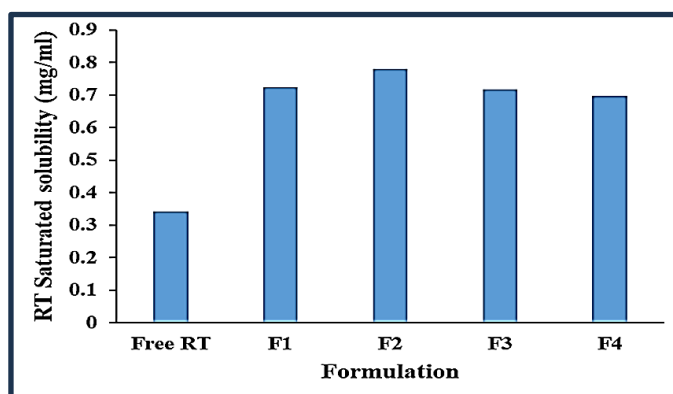


Figure 5. Compares the saturated solubility studies of various RTCPs (F3, F4) and RTNCPs (F1, F2) formulations with Free RT in a phosphate buffer pH 6.8.

These findings suggest that developed F1-F4 formulations had 2.0-2.3-fold higher aqueous solubility than free RT. The degree of solubility enhancement in descending order is F2>F1>F3>F4> free RT.

3.1.7. *In vitro* drug release studies.

Figure 6 shows the cumulative amount of RT release from different RTCPs (F3, F4) and RTNCPs (F1, F2) in comparison to free RT suspension. The drug release data revealed that F1, F2, F3, and F4 formulations exhibited maximum drug release of 72.84±9.93, 62.19±5.99, 51.77±2.99, and 53.02±5.03%, respectively, up to 24 hours. However, an initial burst drug release was observed in 2 hours, followed by a sustained drug release pattern up to 24 hours. Among the various kinetic models tested, the Higuchi model exhibited the highest correlational coefficient (R^2) values for F1, F2, F3, and F4 formulations (Table 4).

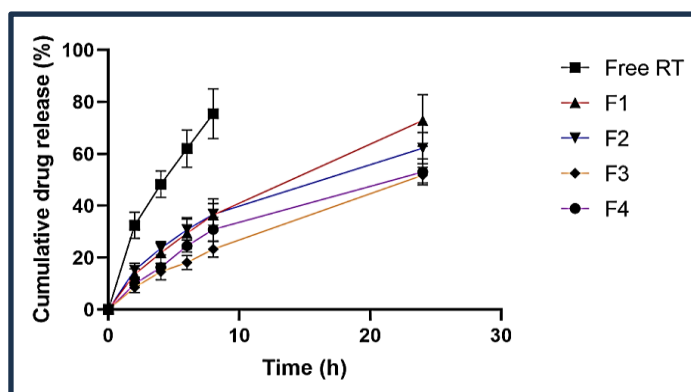


Figure 6. Cumulative % of RT release from RTCPs (F3, F4) and RTNCPs (F1, F2) in a phosphate buffer pH 6.8 (40% v/v PEG 400). In comparison to the RTNCPs and free RT suspension, RTCPs demonstrated a more sustained and prolonged drug release status. Each data points are presented as mean± SD (n=3).

Table 4. Correlational coefficient (R^2) of different kinetic models for interpreting the drug release mechanism.

Kinetic models	Zero-order	First order	Higuchi	Korsmeyer-Peppas
R^2 value (F1)	0.9515	0.9519	0.9826	0.085
R^2 value (F2)	0.9106	0.9111	0.9946	0.0836
R^2 value (F3)	0.9449	0.9413	0.9859	0.0011
R^2 value (F4)	0.9187	0.9192	0.9807	0.0684

3.1.8. Preparation and characterization of polymeric hydrogel.

RTCPs were successfully loaded into the polymeric hydrogel using 2% Carbopol 940 as a gelling agent. All hydrogel formulations appeared pale yellow, and their physical

characteristics are summarized in Table 5. pH values were close to the skin pH, and the drug content ranged from $82\pm 5.6\%$ to $99\pm 2.4\%$ (Table 5). The consistency of the marketed gel was 5.8 ± 0.6 mm, while the formulated hydrogels (MGH1 to MGH3) ranged from 5.3 ± 0.8 mm to 5.6 ± 0.6 mm. Hence, the consistency of the developed hydrogel formulations was better than that of the marketed gel. The gel strength of the prepared MGH1, MGH2, and MGH3 hydrogels was 80 ± 4 s, 85 ± 3 s, and 95 ± 8 s, respectively, while the marketed gel was 75 ± 6 s. These findings suggest that prepared hydrogels have higher gel strength than the marketed gel. Viscosities and spreadabilities of all hydrogel formulations are given in Table 5.

Table 5. Characterization of various polymeric hydrogel formulations. All data are presented as mean \pm SD (n=3).

Formulations	pH	Spreadability (gm. cm/sec)	Viscosity (cPs)	Drug content (%)	Physical appearance
MGH1	4.65 ± 0.32	18.75 ± 2.1	7680 ± 12	99 ± 2.4	Pale yellow color, homogeneous
MGH2	5.17 ± 0.12	12.10 ± 1.21	7097 ± 16	82 ± 5.6	Pale yellow color, homogeneous
MGH3	5.45 ± 0.24	15.51 ± 1.1	6880 ± 10	87 ± 4.7	Pale yellow color, homogeneous

3.1.9. *Ex vivo* skin permeation studies.

Figure 7 shows the cumulative amount of RT permeated through the rat's abdominal skin after 24 hours using the selected free RT hydrogel (MGH1), RTCPs-loaded hydrogel (MGH3), and RTNCPs-loaded hydrogel (MGH2). RTCPs-loaded hydrogel exhibited significantly higher drug permeation (604.33 ± 23.16 $\mu\text{g}/\text{cm}^2$) than the RTNCPs-loaded hydrogel (409.35 ± 35.68 $\mu\text{g}/\text{cm}^2$) and free RT hydrogel (218.97 ± 24.14 $\mu\text{g}/\text{cm}^2$). Flux was measured by comparing the amount of drug permeated vs. time. RTCPs-loaded hydrogel (0.4010 ± 0.03 $\text{mg}/\text{cm}^2/\text{h}$) had 1.39-fold higher permeation flux than the RTNCPs-loaded hydrogel (0.2872 ± 0.01 $\text{mg}/\text{cm}^2/\text{h}$) and 6.47-fold higher than the free RT hydrogel (0.0620 ± 0.01 $\text{mg}/\text{cm}^2/\text{h}$). Apparent permeability coefficients (P_{app}) for RTCPs-loaded hydrogel, RTNCPs-loaded hydrogel, and free RT hydrogel were found to be 0.086 ± 0.02 cm/h , 0.062 ± 0.09 cm/h , 0.013 ± 0.01 cm/h , respectively. All the skin permeation parameters for the various formulations are presented in the supplementary data (Table S2).

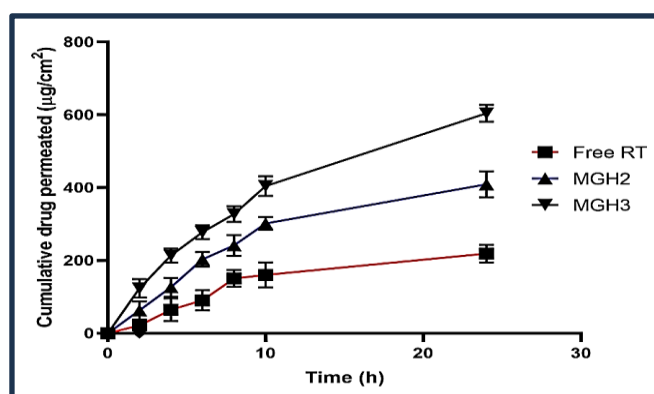


Figure 7. The cumulative amount of RT permeated per unit surface area of rat abdominal skin ($\mu\text{g}/\text{cm}^2$) for free RT hydrogel, RTNCPs-loaded hydrogel (MGH2), and RTCPs-loaded hydrogel (MGH3). The RTCPs-loaded hydrogel showed higher skin permeability than the hydrogel containing free RT and RTNCPs. All data are presented as mean \pm SD (n=3).

3.1.10. Skin retention studies.

After determining the skin permeation profile, the amount of RT retained in the skin was determined spectrophotometrically. The skin retention of RT from the free RT hydrogel, RTNCPs-loaded hydrogel, and RTCPs-loaded hydrogel was found to be 11.54 ± 1.54 %, 40.65 ± 1.00 %, and 52.43 ± 1.32 % of drug content, respectively. These results suggested that RTCPs have higher drug retention than RTNCPs and pure drug RT.

3.1.11. Effect of RTCPs-loaded polymeric hydrogel on the hind paw thickness of FCA-induced rats.

Figure 8 shows the effect on the hind paw thickness of all the group rats. The FCA-induced group of rats showed a significant ($p < 0.005$) increase in paw thickness compared to the normal control rats. The increased paw thickness indicated that inflammation had occurred over the left hind paw of all rats (except normal control rats). This clinical feature of arthritis was gradually reduced after two weeks of topical application of free RT hydrogel, RTCPs-loaded hydrogel, and marketed 1% diclofenac sodium gel to the respective groups of animals. The reduction in paw thickness in the RTCPs-loaded hydrogel-treated group was significantly greater than in the free RT hydrogel and the marketed 1% diclofenac sodium gel-treated groups. These findings suggest that the RTCPs-loaded hydrogel is more effective in reducing paw edema than the commercially available 1% diclofenac sodium gel and free RT hydrogel.

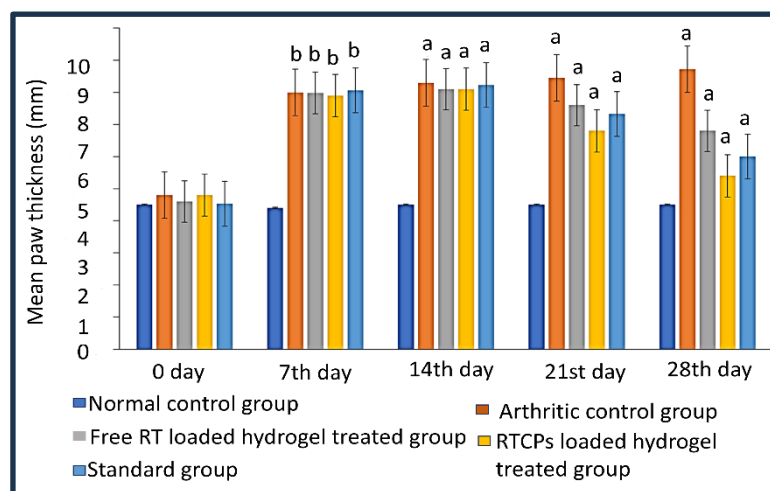


Figure 8. Effect of topical administration of 1% diclofenac sodium gel, RTCPs-loaded hydrogel, and free RT hydrogel after 14th days on increased paw thickness in FCA-induced arthritis rat model. a: significant difference at $P < 0.05$ and b: significant difference at $P < 0.005$. All data are presented as mean \pm SD ($n=4$).

3.1.12. Effect of RTCPs-loaded polymeric hydrogel on the body weight of FCA-induced rats.

Figure 9 illustrates the effect on the body weight of all the rats. The FCA-induced group of rats significantly ($p < 0.005$) reduced body weight compared to the normal control rats. These results suggest that body weight loss occurs during the course of arthritis. However, the body weight of treated animals with free RT hydrogel, RTCPs-loaded hydrogel, and marketed 1% diclofenac sodium gel significantly increased ($p < 0.05$) from days 14 to 28 compared to the arthritic control group. Hence, no significant difference in weight was observed between the normal and treated animal groups.

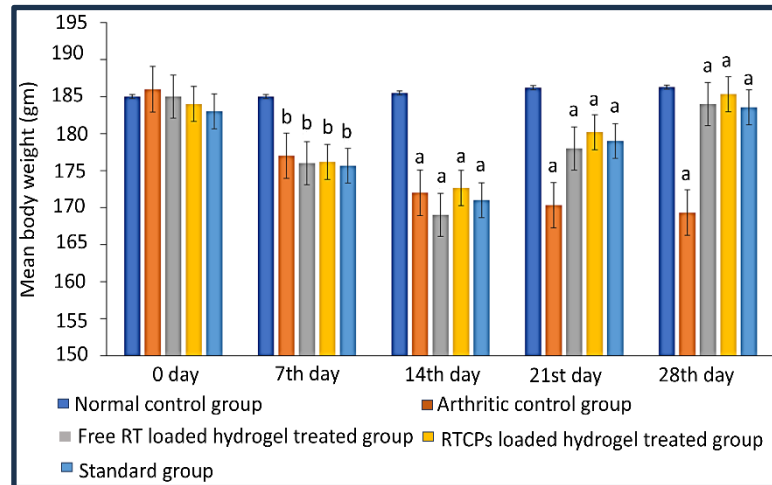


Figure 9. Effect of topical administration of 1% diclofenac sodium gel, RTCPs-loaded hydrogel, and free RT hydrogel after 14th days on decreased body weight in FCA-induced arthritis rat model. a: significant difference at P<0.05 and b: significant difference at P<0.005. All data are presented as mean±SD (n=4).

3.1.13. Hematological parameters.

Table 6 shows changes in hematological parameters across all rat groups. It was observed that arthritic control rats showed a significant ($p < 0.005$) increase in WBC count and a sharp decrease in RBC count compared with normal control rats. However, treatment with RTCP-loaded hydrogel significantly increased RBC count and sharply decreased WBC count compared with arthritic control rats. Similar results were observed in the free RT hydrogel and the marketed 1% diclofenac sodium gel treatment groups.

Table 6. Shows the changes in hematological parameters on topical administration of 1% diclofenac sodium gel, RTCPs-loaded hydrogel, and free RT hydrogel in FCA-induced rats. All data are presented as mean± SD (n=4).

Parameters	Normal control group	Arthritis control group	Free RT hydrogel-treated group	RTCPs-loaded hydrogel-treated group	Standard group
RBC ($\times 10/mm^3$)	5.15±0.01	3.45±0.11	3.94±0.18	4.33±0.01	4.39±0.14
WBC ($\times 10/mm^3$)	8.33±0.13	16.23±0.25	9.12±0.24	10.05±0.13	9.43±0.11

3.1.14. Radiological analysis.

Figure 10 illustrates X-ray radiographs of the left hind paws of all group rats on the last day of the experiment.

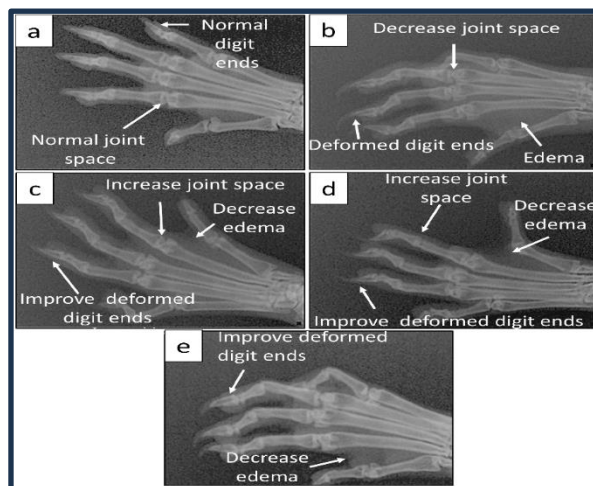


Figure 10. Visual representation of x-ray imaging of different groups: (a) Normal control group; (b) Arthritic control group; (c) Group treated with free RT hydrogel; (d) Group treated with RTCPs-loaded hydrogel; (e) Group treated with marked 1% diclofenac sodium gel.

The swelling of soft tissues around the ankle joints was observed. Still, treatment with RTCPs-loaded hydrogel resulted in significant improvement, as evidenced by radiological parameters including joint space, bone architecture, digit ends, and bone erosion. Similar results were observed in the free RT hydrogel and the marketed 1% diclofenac sodium gel treatment groups.

3.1.15. Histopathological observation.

Figure 11 shows the microscopical examination results of rat paw-skin specimens. The normal control group (Figure 11a) showed normal epidermal layers, whereas the arthritic control group (Figure 11b) showed inflammation, detachment, and ulceration of epidermal layers. The group (Figure 11d) treated with the RTCPs-loaded hydrogel showed less inflammation than the free RT hydrogel (Figure 11c) and the marketed gel-treated group (Figure 11e).

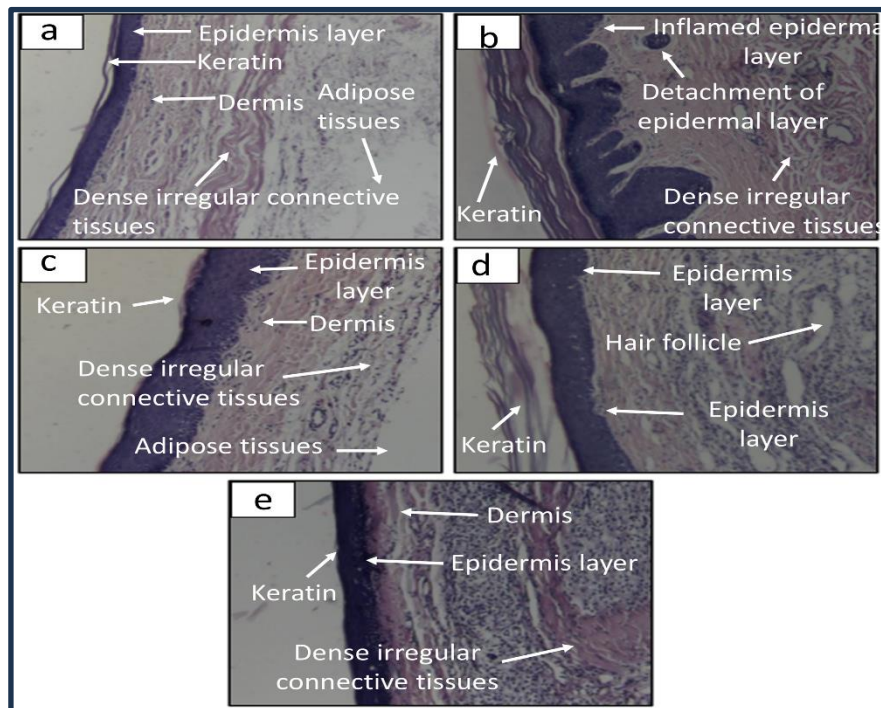


Figure 11. Histopathological observation of rat-paw skin of different groups: (a) Normal control group; (b) Group treated with FCA; (c) Group treated with free RT hydrogel; (d) Group treated with RTCPs-loaded hydrogel; (e) Group treated with marked 1% diclofenac sodium gel.

3.2. Discussion.

The current study focuses on the development of a novel RTCP-loaded polymeric hydrogel that enhances skin permeability and the therapeutic efficacy of RT in RA treatment. After multiple attempts, RTCPs were successfully prepared by a thin-layer hydration method with various molar ratios of RT to PC and SA. Similarly, RTNCPs were prepared without SA. In this formulation, PC interacts with the RT molecules to form complexes (phytosomes) [49], while SA provides a positive charge to the phytosomes' surface. The F3 formulation was selected as the optimized RTCP based on PS, PDI, ZP, and DEE among the formulations. The PS of optimized RTCPs was found to be 527.6 nm, with a narrow PDI of 0.348. This narrow PS is easily permeable through the skin membrane. This argument is supported by previous studies that reported that phytosomes with a PS of 1160 nm can easily penetrate the skin membrane [50]. The low PDI indicated a narrow PS distribution, suitable for topical

administration. Moreover, varied molar ratios RT to PC and SA content had a substantial effect on PS, PDI, and ZP as well. We observed that the PS and PDI of the F1 and F2 formulations decreased as the PC molar ratio increased. This may be achieved by increasing the molar ratio of PC, allowing more drug to embed within the phospholipid bilayer and resulting in fewer RT molecules in contact during complex formation. However, the PS of F3 and F4 formulations increases as the molar ratio of SA content increases. It may be attributed to the high concentration of SA inclusion in phytosomes, acting as a charge inducer, which altered the spacing between adjacent bilayers [51]. Similarly, ZP values of formulated phytosomes decrease as the molar ratio of PC content increases, which is due to PC's negative charge (phosphate group) [52], whereas SA increases ZP values due to its cationic charge. Nonetheless, the ZP value of optimized RTCPs (F3) indicated good colloidal stability, as nanoformulations with ZP values of ± 25 mV are generally considered to exhibit high colloidal stability [53]. The DEE and DL are two important key parameters that assisted in determining the total amount of drug feed during phytosomes formulation [54]. The obtained results (Table 3) demonstrated that RTCPs have higher DEE and DL than RTNCPs. However, the DEE and DL of the RTCPs significantly decreased when the SA content molar ratio exceeded 4.96 (F4). These findings suggest that optimal concentration of SA aids in DEE and DL, as discussed in previous research [55].

FT-IR and DSC analysis helped in assessing the drug excipient's compatibility and its complex formation [56]. We observed that the FT-IR spectra of the individual components (RT, PC, and SA) and their physical mixture exhibited all the absorption band characteristics without any notable variations, thus proving their compatibility. However, the intensity of the O-H peak of both RTCPs and RTNCPs was reduced when compared to pure drug RT, thus confirming the complexation formed between RT and PC via hydrogen bonding [57]. This fact is further supported by DSC analysis. DSC thermogram of RT showed two broad endothermic peaks at 154.26°C and 179.17°C, respectively. The endothermic peak at 179.17°C corresponded to the melting point of RT [58]. The endothermic peak at 154.26°C was attributed to the dehydration of RT [59]. All endothermic peak characteristics of the physical mixture and its components were retained with minor variations, thus confirming their compatibility. Interestingly, the absence of RT endothermic peaks in the DSC thermograms of RTCPs and RTNCPs indicates that RT was completely embedded within the phospholipid matrix.

The HR-TEM images of RTCPs (F3) and RTNCPs (F2) revealed the formation of distinct vesicle shapes, homogeneity, and no aggregation (Figure 4). The internal diameters of the RTCPs and RTNCPs were obtained within the range of DLS data. Furthermore, HR-TEM images reveal numerous small, white, and dense spherical-shaped bodies that are rutin-loaded complexes covered by the lipid vesicle. Hence, the above findings confirmed that RT was completely loaded into the phospholipid matrix [60]. Solubility data revealed that RTCPs (F3, F4) are more soluble than free RT but slightly less soluble than RTNCPs (F1, F2). This finding suggests that SA may be attributed to the cationic charge in phospholipid complexes, leading to decreased solubility. This argument is further supported by *in vitro* drug release data. We observed that RTCPs and RTNCPs have an initial burst drug release in 2 hours, followed by a sustained drug release pattern up to 24 hours. Moreover, RTCPs exhibited a more sustained and slower drug release status. It may be attributed to the inclusion of the SA charge in phytosomes, which act as a physical barrier to drug diffusion, resulting in slower and more sustained release of the encapsulated drug from the phytosomes cores [61]. Furthermore, *in vitro drug release data evaluated using various kinetic models indicated that RT release from*

RTCPs and RTNCPs followed a diffusion-controlled mechanism. In addition to this, RTCPs exhibited greater stability in both normal and refrigerated conditions than RTNCPs. This may be achieved due to the cationic charge of phytosomes, which repel each other enough to maintain stability.

Topical polymeric hydrogels were prepared by mixing optimized RTCPs with 2% (w/v) Carbopol 940 gelling agent, as shown in Table 2. All developed hydrogel formulations exhibited a pale yellow color, were free of grittiness, and had a smooth appearance without greasiness on application. Hydrogel pH values were found to be close to the skin pH, which is acceptable for topical application without any risk of skin irritation [62]. The consistency reflects the gel's capacity to be ejected uniformly and in the desired quantity when the tube is squeezed. The consistency of the developed hydrogel formulations was found to be better than that of the marketed gel. Gel strength is a measure of a colloidal dispersion's ability to form and sustain a gel form. Strong gels will withstand far greater pressure than weaker gels before being flushed from the site of administration, and this will also affect the spreadability [63]. All developed hydrogel formulations showed good gel strength and met the ideal quality requirements for topical application. Viscosity is an important physical parameter in topical formulations and affects their spreadability and drug release rate [64]. However, the viscosity of all developed hydrogel formulations (MGH1 to MGH3) was found to be within the desired range of 2000-4000 cPs [65]. The spreadability data indicate that the hydrogel is easily spreadable by a small amount of shear. It was considered an important factor in improving patient compliance during treatment [66]. Drug content data for polymeric hydrogels indicate that RTCPs, RTNCPs, and free RT are uniformly distributed in Carbopol gels, with minimal losses throughout the formulation process. Further, *ex vivo* permeation data showed that RTCPs-loaded hydrogel had 1.39-fold higher permeability than RTNCPs-loaded hydrogel and 6.47-fold higher permeability than free RT hydrogel. This is accomplished by incorporating RTCPs (F3) into the polymeric hydrogel, which readily internalizes into negatively charged skin cells, thereby increasing skin permeability, as discussed in previous research [67, 68]. Interestingly, RTCPs-loaded hydrogel also demonstrated superior skin retention when compared to hydrogel containing RTNCPs and free RT. This might be achieved due to the cationic charge effect of SA that alters the tight junction of the stratum corneum layer, allowing the drug to easily permeate through the stratum corneum and remain in the skin layers to form a drug reservoir, resulting in a slow-release effect and achieving the full therapeutic potential for RA [69].

In vivo anti-arthritic studies on FCA-induced rats demonstrated that hydrogel-containing RTCPs had a greater inhibitory effect on paw edema than the free RT hydrogel and the marketed gel-treated groups. This may be accomplished by increasing skin permeability and by accumulating more RTCPs at sites of inflammation. The argument is supported by previous research showing that cationic liposomes exhibit greater permeation and accumulation than anionic liposomes [70]. Furthermore, the FCA-induced group of rats demonstrated a significant reduction in body weight as compared to the normal control rats. This is attributed to impaired intestinal absorption of food intake during arthritic inflammation. Previous studies have also reported that body weight loss occurs during arthritis [71]. However, rats treated with RTCP-loaded hydrogel, free RT hydrogel, and marketed gel showed significantly increased body weight compared with arthritic control rats. This may be achieved through the intestinal protective action of RT [72], which restored impaired intestinal absorption and prevented weight loss.

Hematological alterations are the key signs of immune system abnormalities in RA patients [70]. In the present study, WBC count significantly increased while RBC count sharply decreased in the arthritic control group. The increased WBC count was linked to immune system stimulation against invading antigens, whereas the reduced RBC count was due to anemia in arthritic rats [73]. However, the treatment groups dramatically restored RBC and WBC to near-normal levels. Hence, its significance in arthritis conditions is justified.

During arthritis, the spacing between joints gets reduced due to cartilage damage, bone erosion, and infiltration of inflammatory mediators [74]. However, X-ray analysis revealed that the group treated with a loaded hydrogel showed significant improvements in radiological parameters, including joint space, bone architecture, digit ends, and bone erosion, thus confirming the protective effect of RT against inflammation-related joint changes. Furthermore, histopathological data revealed that the group treated with RTCPs-loaded hydrogel showed significant improvement in inflammatory skin tissues and the structural integrity of epidermal layers. This may be achieved through better penetration and higher retention of RT across different skin layers, which is further attributed to its extended anti-inflammatory effects in superficial and deep skin layers, the bone interlocks, and adjacent muscular tissues, providing relief in arthritis.

4. Conclusions

This study demonstrated that RTCPs were successfully prepared via thin-layer hydration and exhibited excellent drug entrapment efficiency and loading capacity, as well as uniform, spherical morphologies. The results for drug-excipient compatibility, stability, and surface properties of RTCPs were within the acceptable range. *In vitro* drug release studies revealed sustained release of rutin from the RTCPs over 24 hours, following Higuchi release kinetics. It explains that the mechanisms of rutin release from the RTCPs were diffusion-controlled. Further, RTCPs (F3) were incorporated into polymeric hydrogels convenient for topical application on FCA-induced rats. The findings of *ex vivo* skin permeation and drug retention studies of RTCPs-loaded hydrogel (MGH3) revealed higher skin permeability and drug retention than those of hydrogel containing free RT and RTNCPs. The results of *in vivo* anti-arthritic studies demonstrated a significant decrease in paw edema thickness and increased body weight in FCA-induced rats after topical application of RTCPs-loaded hydrogel.

Furthermore, the RTCPs-loaded hydrogel-treated group demonstrated significant improvements in hematological and radiological parameters compared to the groups receiving free RT hydrogel and the marketed gel. Histopathological studies demonstrated that RTCP-loaded hydrogel could restore affected animals to normal and eliminate arthritis symptoms. Therefore, it can be concluded that the developed RTCP-loaded hydrogel is a superior alternative nanocarrier for treating RA and possibly other inflammatory diseases. However, further studies are warranted to determine its clinical translation from lab to clinic.

Author Contributions

Conceptualization, M.K.D.; methodology, S.D.; software, S.D.; validation, M.K.D., S.D., and S.D.; formal analysis, S.D.; investigation, M.K.D.; resources, S.D.; data curation, M.K.D.; writing—original draft preparation, S.D.; writing—review and editing, L.R.S.; visualization, P.D.; supervision, M.K.D. All authors have read and agreed to the published version of the manuscript.

Institutional Review Board Statement

The animal study protocol was approved in accordance with the Institutional Animal Ethical Committee (IAEC) guidelines of the Department of Pharmaceutical Sciences, Dibrugarh University, Dibrugarh, Assam, India, under Approval No. IAEC/DU/202, Dated. 19/05/2021.

Informed Consent Statement

Not applicable.

Data Availability Statement

Data supporting the findings of this study are available upon reasonable request from the corresponding author.

Funding

This work was financially supported by the All India Council for Technical Education (AICTE)-PG Scholarship Scheme.

Acknowledgments

The authors are thankful to the Drug Delivery Research Laboratory (DDRL), Department of Pharmaceutical Sciences, Dibrugarh University, Dibrugarh, Assam, India, for providing the platform to conduct this work.

Conflicts of Interest

The authors declare that they have no conflict of interest. All the tables and figures are original and self-made.

References

1. Kakehasi, A.M.; Duarte, A.L.B.P.; Brenol, C.V.; Domiciano, D.S.; Laurindo, I.M.M.; Bonfiglioli, K.R.; da Mota, L.M.H.; Buch, M.H.; de Almeida Macêdo, E.; Xavier, R.M. Challenges in implementing treat-totarget in rheumatoid arthritis: a perspective from Brazilian rheumatologists. *Adv Rheumatol.* **2024**, *64*, 63, <https://doi.org/10.1186/s42358-024-00403-w>.
2. Zheng, M.; Jia, H.; Wang, H.; Liu, L.; He, Z.; Zhang, Z.; Yang, W.; Gao, L.; Gao, X.; Gao, F. Application of nanomaterials in the treatment of rheumatoid arthritis. *RSC Adv.* **2021**, *11*, 7129-7137, <https://doi.org/10.1039/d1ra00328c>.
3. Janakiraman, K.; Krishnaswami, V.; Rajendran, V.; Natesan, S.; Kandasamy, R. Novel nano therapeutic materials for the effective treatment of rheumatoid arthritis-recent insights. *Mater. Today Commun.* **2018**, *17*, 200-213, <https://doi.org/10.1016/j.mtcomm.2018.09.011>.
4. Karami, J.; Aslani, S.; Jamshidi, A.; Garshasbi, M.; Mahmoudi, M. Genetic implications in the pathogenesis of rheumatoid arthritis; an updated review. *Gene* **2019**, *702*, 8-16, <https://doi.org/10.1016/j.gene.2019.03.033>.
5. Padyukov, L. Genetics of rheumatoid arthritis. *Semin. Immunopathol.* **2022**, *44*, 47-62, <https://doi.org/10.1007/s00281-022-00912-0>.
6. Harirforoosh, S.; Asghar, W.; Jamali, F. Adverse Effects of Nonsteroidal Anti-inflammatory Drugs: An Update of Gastrointestinal, Cardiovascular and Renal Complications. *J. Pharm. Pharm. Sci.* **2014**, *16*, 821-847, <https://doi.org/10.18433/j3vw2f>.
7. Haroutiunian, S.; Drennan, D.A.; Lipman, A.G. Topical NSAID Therapy for Musculoskeletal Pain. *Pain Med.* **2010**, *11*, 535-549, <https://doi.org/10.1111/j.1526-4637.2010.00809.x>.

8. Barkin, R.L. Topical Nonsteroidal Anti-inflammatory Drugs: The Importance of Drug, Delivery, and Therapeutic Outcome. *Am. J. Ther.* **2015**, *22*, 388-407, <https://doi.org/10.1097/mjt.0b013e3182459abd>.
9. Bobek, D.; Stipetić, A.B.; Franić, M.; Lucijanić, M.; Lucijanić, J.; Gračanin, A.G.; Mijačika, L.; Perić, P. Use of Nonsteroidal Anti-inflammatory Drugs in Patients with Advanced Active Rheumatoid Arthritis. *Acta Clin. Croat.* **2022**, *61*, 588-597, <https://doi.org/10.20471/acc.2022.61.04.04>.
10. Singh, G. Recent considerations in nonsteroidal anti-inflammatory drug gastropathy. *Am. J. Med.* **1998**, *105*, 31S-38S, [https://doi.org/10.1016/s0002-9343\(98\)00072-2](https://doi.org/10.1016/s0002-9343(98)00072-2).
11. McCarberg, B.; D'Arcy, Y. Options in Topical Therapies in the Management of Patients With Acute Pain. *Postgrad. Med.* **2013**, *125*, 19-24, <https://doi.org/10.1080/00325481.2013.1110567011>.
12. Derry, S.; Conaghan, P.; Da Silva, J.A.P.; Wiffen, P.J.; Moore, R.A. Topical NSAIDs for chronic musculoskeletal pain in adults. *Cochrane Database Syst. Rev.* **2016**, *2016*, CD007400, <https://doi.org/10.1002/14651858.cd007400.pub3>.
13. McPherson, M.L.; Cimino, N.M. Topical NSAID Formulations. *Pain Med.* **2013**, *14*, S35-S39, <https://doi.org/10.1111/pme.12288>.
14. Makris, U.E.; Kohler, M.J.; Fraenkel, L. Adverse Effects of Topical Nonsteroidal Anti-inflammatory Drugs in Older Adults with Osteoarthritis: A Systematic Literature Review. *J. Rheumatol.* **2010**, *37*, 1236-1243, <https://doi.org/10.3899/jrheum.090935>.
15. Sharma, D.; Chaubey, P.; Suvarna, V. Role of natural products in alleviation of rheumatoid arthritis-A review. *J. Food Biochem.* **2021**, *45*, e13673, <https://doi.org/10.1111/jfbc.13673>.
16. Umar, S.; Mishra, N.K.; Kaushal, P.; Sajad, M.; Neha; Ansari, M.M.; Ahmad, S.; Katiyar, C.K.; Khan, H.A. Protective effect of rutin in attenuation of collagen-induced arthritis in Wistar rat by inhibiting inflammation and oxidative stress. *Indian J. Rheumatol.* **2012**, *7*, 191-198, <https://doi.org/10.1016/j.injr.2012.09.001>.
17. Das, M.K.; Kalita, B. Design and Evaluation of Phyto-Phospholipid Complexes (Phytosomes) of Rutin for Transdermal Application. *Appl. Pharm. Sci.* **2014**, *4*, 51-57, <https://doi.org/10.7324/japs.2014.401010>.
18. Gul, A.; Kunwar, B.; Mazhar, M.; Faizi, S.; Ahmed, D.; Shah, M.R.; Simjee, S.U. Rutin and rutin-conjugated gold nanoparticles ameliorate collagen-induced arthritis in rats through inhibition of NF- κ B and iNOS activation. *Int. Immunopharmacol.* **2018**, *59*, 310-317, <https://doi.org/10.1016/j.intimp.2018.04.017>.
19. Choi, K.-S.; Kundu, J.K.; Chun, K.-S.; Na, H.-K.; Surh, Y.-J. Rutin inhibits UVB radiation-induced expression of COX-2 and iNOS in hairless mouse skin: p38 MAP kinase and JNK as potential targets. *Arch. Biochem. Biophys.* **2014**, *559*, 38-45, <https://doi.org/10.1016/j.abb.2014.05.016>.
20. Ostrakhovitch, E.A.; Afanas'ev, I.B. Oxidative stress in rheumatoid arthritis leukocytes: suppression by rutin and other antioxidants and chelators. *Biochem. Pharmacol.* **2001**, *62*, 743-746, [https://doi.org/10.1016/s0006-2952\(01\)00707-9](https://doi.org/10.1016/s0006-2952(01)00707-9).
21. Li, J.; Ni, W.; Aisha, M.; Zhang, J.; Sun, M. A rutin nanocrystal gel as an effective dermal delivery system for enhanced anti-photoaging application. *Drug Dev. Ind. Pharm.* **2021**, *47*, 429-439, <https://doi.org/10.1080/03639045.2021.1890113>.
22. Semalty, A.; Semalty, M.; Rawat, M.S.M.; Franceschi, F. Supramolecular phospholipids–polyphenolics interactions: The PHYTOSOME® strategy to improve the bioavailability of phytochemicals. *Fitoterapia* **2010**, *81*, 306-314, <https://doi.org/10.1016/j.fitote.2009.11.001>.
23. Alharbi, W.S.; Almughem, F.A.; Almeahmady, A.M.; Jarallah, S.J.; Alsharif, W.K.; Alzahrani, N.M.; Alshehri, A.A. Phytosomes as an Emerging Nanotechnology Platform for the Topical Delivery of Bioactive Phytochemicals. *Pharmaceutics* **2021**, *13*, 1475, <https://doi.org/10.3390/pharmaceutics13091475>.
24. Kalita, B.; Das, M.K. Rutin–phospholipid complex in polymer matrix for long-term delivery of rutin via skin for the treatment of inflammatory diseases. *Artif. Cells Nanomed. Biotechnol.* **2018**, *46*, 41-56, <https://doi.org/10.1080/21691401.2017.1411931>.
25. Wanjiru, J.; Gathirwa, J.; Sauli, E.; Swai, H.S. Formulation, Optimization, and Evaluation of *Moringa oleifera* Leaf Polyphenol-Loaded Phytosome Delivery System against Breast Cancer Cell Lines. *Molecules* **2022**, *27*, 4430, <https://doi.org/10.3390/molecules27144430>.
26. González-Rodríguez, M.; Rabasco, A.M. Charged liposomes as carriers to enhance the permeation through the skin. *Expert Opin. Drug Deliv.* **2011**, *8*, 857-871, <https://doi.org/10.1517/17425247.2011.574610>.
27. Dragicevic-Curic, N.; Gräfe, S.; Gitter, B.; Winter, S.; Fahr, A. Surface charged temoporfin-loaded flexible vesicles: *In vitro* skin penetration studies and stability. *Int. J. Pharm.* **2010**, *384*, 100-108, <https://doi.org/10.1016/j.ijpharm.2009.10.006>.

28. Duangjit, S.; Opanasopit, P.; Rojanarata, T.; Ngawhirunpat, T. Evaluation of Meloxicam-Loaded Cationic Transfersomes as Transdermal Drug Delivery Carriers. *AAPS PharmSciTech* **2013**, *14*, 133-140, <https://doi.org/10.1208/s12249-012-9904-2>.
29. Babazadeh, A.; Ghanbarzadeh, B.; Hamishehkar, H. Phosphatidylcholine-rutin complex as a potential nanocarrier for food applications. *J. Funct. Foods* **2017**, *33*, 134-141, <https://doi.org/10.1016/j.jff.2017.03.038>.
30. Rasaie, S.; Ghanbarzadeh, S.; Mohammadi, M.; Hamishehkar, H. Nano Phytosomes of Quercetin: A Promising Formulation for Fortification of Food Products with Antioxidants. *Pharm. Sci.* **2014**, *20*, 96-101.
31. Diño, S.F.; Edu, A.D.; Francisco, R.G.; Gutierrez, E.; Crucis, P.; Lapuz, A.M.; Carandang, R.R.; Miranda, K.J. Drug-Excipient Compatibility Testing of Cilostazol Using FTIR and DSC Analysis. *Philipp. J. Sci.* **2023**, *152*, 2129-2137.
32. Jain, S.; Jain, P.; Umamaheshwari, R.B.; Jain, N.K. Transfersomes—A Novel Vesicular Carrier for Enhanced Transdermal Delivery: Development, Characterization, and Performance Evaluation. *Drug Dev. Ind. Pharm.* **2003**, *29*, 1013-1026, <https://doi.org/10.1081/ddc-120025458>.
33. Kumar, L.; Suhas, B.S.; Pai, G.K.; Verma, R. Determination of Saturated Solubility of Naproxen using UV Visible Spectrophotometer. *Res. J. Pharm. Technol.* **2015**, *8*, 825-828, <https://doi.org/10.5958/0974-360x.2015.00134.1>.
34. Wolska, E.; Szymańska, M. Comparison of the In Vitro Drug Release Methods for the Selection of Test Conditions to Characterize Solid Lipid Microparticles. *Pharmaceutics* **2023**, *15*, 511, <https://doi.org/10.3390/pharmaceutics15020511>.
35. Dave, V.; Sharma, S.; Yadav, R.B.; Agarwal, U. Herbal liposome for the topical delivery of ketoconazole for the effective treatment of seborrheic dermatitis. *Appl. Nanosci.* **2017**, *7*, 973-987, <https://doi.org/10.1007/s13204-017-0634-3>.
36. Abbas, K.; Amin, A.; Mudassir, J.; Abdullah Alzahrani, A.Y.; Saher, T.; Manzoor, R.; Aleem, A.; Khan, M.A.; Wazir, M.A.; Rana, S.J.; Abdul khaliq, H.; Usman, A.; Sial, A.S.; Zia ul Hasnain, S. Preparation, characterization and evaluation of hydrogels from different fractions of diverse medicinal plants for management of pain and inflammation. *Int. J. Food Prop.* **2023**, *26*, 2532-2552, <https://doi.org/10.1080/10942912.2023.2250572>.
37. El-Housiny, S.; Shams Eldeen, M.A.; El-Attar, Y.A.; Salem, H.A.; Attia, D.; Bendas, E.R.; El-Nabarawi, M.A. Fluconazole-loaded solid lipid nanoparticles topical gel for treatment of pityriasis versicolor: formulation and clinical study. *Drug Deliv.* **2018**, *25*, 78-90, <https://doi.org/10.1080/10717544.2017.1413444>.
38. Ayoub, R.K.; Murtaza, G.; Imran, M.; Khan, S.A.; Mir, S.; Khan, A.K.; Azhar, S.; Mehmood, Z.; Sajjad, A.; Shah, S.N.H. Formulation and permeation kinetic studies of flurbiprofen gel. *Trop. J. Pharm. Res.* **2015**, *14*, 195-203, <https://doi.org/10.4314/tjpr.v14i2.2>.
39. Pandit, A.P.; Pol, V.V.; Kulkarni, V.S. Xyloglucan Based In Situ Gel of Lidocaine HCl for the Treatment of Periodontosis. *J. Pharm.* **2016**, *2016*, 3054321, <https://doi.org/10.1155/2016/3054321>.
40. Aiyalu, R.; Govindarjan, A.; Ramasamy, A. Formulation and evaluation of topical herbal gel for the treatment of arthritis in animal model. *Braz. J. Pharm. Sci.* **2016**, *52*, 493-507, <https://doi.org/10.1590/s1984-82502016000300015>.
41. Singh, V.K.; Singh, P.K.; Sharma, P.K.; Srivastava, P.K.; Mishra, A. Formulation and evaluation of topical gel of acefenac containing piparine. *Indo Am. J. Pharm. Res.* **2013**, *3*, 5266-5280.
42. Lowanshi, K.; Pawar, R.S. Formulation and evaluation of Ketorolac hydrogel for effective management of dermatitis. *Asian J. Pharm. Pharmacol.* **2023**, *9*, 153-158, <http://dx.doi.org/10.31024/ajpp.2023.9.5.2>.
43. Hassan, A.S.; Soliman, G.M. Rutin Nanocrystals with Enhanced Anti-inflammatory Activity: Preparation and Ex Vivo/In Vivo Evaluation in an Inflammatory Rat Model. *Pharmaceutics* **2022**, *14*, 2727, <https://doi.org/10.3390/pharmaceutics14122727>.
44. Elshall, A.A.; Ghoneim, A.M.; Abdel-Mageed, H.M.; Osman, R.; Shaker, D.S. Ex vivo permeation parameters and skin deposition of melatonin-loaded microemulsion for treatment of alopecia. *Futur. J. Pharm. Sci.* **2022**, *8*, 28, <https://doi.org/10.1186/s43094-022-00418-4>.
45. Gautam, R.K.; Sharma, S.; Sharma, K.; Gupta, G. Evaluation of Antiarthritic Activity of Butanol Fraction of *Punica granatum* Linn. Rind Extract Against Freund's Complete Adjuvant-Induced Arthritis in Rats. *J. Environ. Pathol. Toxicol. Oncol.* **2018**, *37*, 53-62, <https://doi.org/10.1615/jenvironpatholtoxicoloncol.2018025137>.

46. Sharma, V.; Shukla, S.S.; Gidwani, B.; Pandey, R.K. Antiarthritic Activity and Inflammatory Mediators Modulation Effect of Traditional Ajmodadi Churna on Arthritis Experimental Model. *J. Pharmacopunct.* **2023**, *26*, 257-264, <https://doi.org/10.3831%2FKPI.2023.26.3.257>.
47. Khan, D.; Qindeel, M.; Ahmed, N.; Khan, A.U.; Khan, S.; Rehman, A.U. Development of Novel Ph-Sensitive Nanoparticle-Based Transdermal Patch for Management of Rheumatoid Arthritis. *Nanomedicine* **2020**, *15*, 603-624, <https://doi.org/10.2217/nnm-2019-0385>.
48. Eltobshi, A.A.; Mohamed, E.A.; Abdelghani, G.M.; Nouh, A.T. Self-nanoemulsifying drug-delivery systems for potentiated anti-inflammatory activity of diacerein. *Int. J. Nanomed.* **2018**, *13*, 6585-6602, <https://doi.org/10.2147/ijn.s178819>.
49. Gnananath, K.; Nataraj, K.S.; Rao, B.G. Phospholipid Complex Technique for Superior Bioavailability of Phytoconstituents. *Adv. Pharm. Bull.* **2017**, *7*, 35-42, <https://doi.org/10.15171/apb.2017.005>.
50. Kalita, B.; Das, M.K. Resveratrol-phospholipid complexes (phytosomes) with improved physicochemical properties favorable for drug delivery via skin. *World J. Pharm. Res.* **2015**, *4*, 1497-1517.
51. Ghule, M.M.; Bhojar, G.S. Formulation and Evaluation of Modified Liposome for Transdermal Drug. *J. Dev. Drugs* **2018**, *7*, 186, <http://dx.doi.org/10.4172/2329-6631.1000186>.
52. Pasenkiewicz-Gierula, M.; Takaoka, Y.; Miyagawa, H.; Kitamura, K.; Kusumi, A. Charge Pairing of Headgroups in Phosphatidylcholine Membranes: A Molecular Dynamics Simulation Study. *Biophys. J.* **1999**, *76*, 1228-1240, [https://doi.org/10.1016/s0006-3495\(99\)77286-3](https://doi.org/10.1016/s0006-3495(99)77286-3).
53. Sarma, S.; Agarwal, S.; Bhuyan, P.; Hazarika, J.; Ganguly, M. Resveratrol-loaded chitosan-pectin core-shell nanoparticles as novel drug delivery vehicle for sustained release and improved antioxidant activities. *R. Soc. Open Sci.* **2022**, *9*, 210784, <https://doi.org/10.1098/rsos.210784>.
54. Jaiswal, P.K.; Das, S.; Das, M.K. Boosting the skin delivery of curcumin through stearic acid-ethyl cellulose blend hybrid nanocarriers-based approach for mitigating psoriasis. *Int. J. Appl. Pharm.* **2021**, *13*, 150-164, <https://doi.org/10.22159/ijap.2021v13i3.40668>.
55. Sant, V.; Paradkar, A.R.; Nagarsenker, M. Optimization of pentoxifylline liposomes using 24 factorial design. *Indian J. Pharm. Sci.* **2002**, *64*, 459-464.
56. Pani, N.R.; Nath, L.K.; Acharya, S.; Bhuniya, B. Application of DSC, IST, and FTIR study in the compatibility testing of nateglinide with different pharmaceutical excipients. *J. Therm. Anal. Calorim.* **2012**, *108*, 219-226, <https://doi.org/10.1007/s10973-011-1299-x>.
57. Anwar, E.; Farhana, N. Formulation and Evaluation of Phytosome-Loaded Maltodextrin-Gum Arabic Microsphere System for Delivery of Camellia sinensis Extract. *J. Young. Pharm.* **2018**, *10*, S56-S62, <https://doi.org/10.5530/jyp.2018.2s.11>.
58. Asfour, M.H.; Mohsen, A.M. Formulation and evaluation of pH-sensitive rutin nanospheres against colon carcinoma using HCT-116 cell line. *J. Adv. Res.* **2018**, *9*, 17-26, <https://doi.org/10.1016/j.jare.2017.10.003>.
59. Ismail, A.; El-Biyally, E.; Sakran, W. An Innovative Approach for Formulation of Rutin Tablets Targeted for Colon Cancer Treatment. *AAPS PharmSciTech* **2023**, *24*, 68, <https://doi.org/10.1208/s12249-023-02518-7>.
60. Rahman, M.; Singh, J.G.; Afzal, O.; Altamimi, A.S.A.; Alrobaian, M.; Haneef, J.; Barkat, M.A.; Almalki, W.H.; Handa, M.; Shukla, R.; Nasar Mir Najib Ullah, S.; Kumar, V.; Beg, S. Preparation, Characterization, and Evaluation of Curcumin-Graphene Oxide Complex-Loaded Liposomes against *Staphylococcus aureus* in Topical Disease. *ACS Omega* **2022**, *7*, 43499-43509, <https://doi.org/10.1021/acsomega.2c03940>.
61. Hou, Z.; Li, Y.; Huang, Y.; Zhou, C.; Lin, J.; Wang, Y.; Cui, F.; Zhou, S.; Jia, M.; Ye, S.; Zhang, Q. Phytosomes Loaded with Mitomycin C-Soybean Phosphatidylcholine Complex Developed for Drug Delivery. *Mol. Pharmaceutics* **2013**, *10*, 90-101, <https://doi.org/10.1021/mp300489p>.
62. Lukić, M.; Pantelić, I.; Savić, S.D. Towards Optimal pH of the Skin and Topical Formulations: From the Current State of the Art to Tailored Products. *Cosmetics* **2021**, *8*, 69, <https://doi.org/10.3390/cosmetics8030069>.
63. Bayan M.F.; Chandrasekaran, B.; Alyami, M.H. Development and Characterization of Econazole Topical Gel. *Gels* **2023**, *9*, 929, <https://doi.org/10.3390/gels9120929>.
64. Singh M.P.; Nagori, B.P.; Shaw, N.R.; Tiwari, M.; Jhanwar, B. Formulation Development & Evaluation of Topical Gel Formulations Using Different Gelling Agents and Its Comparison with Marketed Gel Formulation. *Int. J. Pharm. Erudition* **2013**, *3*, 1-10.
65. Sagala, R.J.; Kambira, P.F.A.; Gunawan, U.; Pollin, G. IAI SPECIAL EDITION: The potential of citronella grass to inhibit growth of *Escherichia coli* and *Staphylococcus aureus* bacteria. *Pharm. Educ.* **2022**, *22*, 218-224, <https://doi.org/10.46542/pe.2022.222.218224>.

66. Gangurde, A.B.; Amin, P.D. Microencapsulation by Spray Drying of Vitamin A Palmitate from Oil to Powder and Its Application in Topical Delivery System. *J. Encapsul. Adsorpt. Sci.* **2017**, *7*, 10, <https://doi.org/10.4236/jeas.2017.71002>.
67. Farshbaf, M.; Davaran, S.; Zarebkohan, A.; Annabi, N.; Akbarzadeh, A.; Salehi, R. Significant role of cationic polymers in drug delivery systems. *Artif. Cells Nanomed. Biotechnol.* **2018**, *46*, 1872-1891, <https://doi.org/10.1080/21691401.2017.1395344>.
68. Gillet, A.; Compère, P.; Lecomte, F.; Hubert, P.; Ducat, E.; Evrard, B.; Piel, G. Liposome surface charge influence on skin penetration behaviour. *Int. J. Pharm.* **2011**, *411*, 223-231, <https://doi.org/10.1016/j.ijpharm.2011.03.049>.
69. Lin, H.W.; Xie, Q.C.; Huang, X.; Ban, J.F.; Wang, B.; Wei, X.; Chen, Y.Z.; Lu, Z.F. Increased skin permeation efficiency of imperatorin via charged ultradeformable lipid vesicles for transdermal delivery. *Int. J. Nanomed.* **2018**, *13*, 831-842, <https://doi.org/10.2147/ijn.s150086>.
70. baraki, H.; Takeda, A.; Arima, N.; Hatakeyama, N.; Takashima, Y.; Seta, Y.; Kanazawa, T. In Vivo Fluorescence Imaging of Passive Inflammation Site Accumulation of Liposomes via Intravenous Administration Focused on Their Surface Charge and PEG Modification. *Pharmaceutics* **2021**, *13*, 104, <https://doi.org/10.3390/pharmaceutics13010104>.
71. Bihani, G.V.; Rojatkār, S.R.; Bodhankar, S.L. Anti-arthritis activity of methanol extract of *Cyathocline purpurea* (whole plant) in Freund's complete adjuvant-induced arthritis in rats. *Biomed. Aging Pathol.* **2014**, *4*, 197-206, <https://doi.org/10.1016/j.biomag.2014.04.007>.
72. Mascaraque, C.; Aranda, C.; Ocón, B.; Monte, M.J.; Suárez, M.D.; Zarzuelo, A.; Marín, J.J.G.; Martínez-Augustin, O.; de Medina, F.S. Rutin has intestinal anti-inflammatory effects in the CD4+ CD62L+ T cell transfer model of colitis. *Pharmacol. Res.* **2014**, *90*, 48-57, <https://doi.org/10.1016/j.phrs.2014.09.005>.
73. Ekambaram, S.; Perumal, S.S.; Subramanian, V. Evaluation of antiarthritic activity of *Strychnos potatorum* Linn seeds in Freund's adjuvant induced arthritic rat model. *BMC Complement. Altern. Med.* **2010**, *10*, 56, <https://doi.org/10.1186/1472-6882-10-56>.
74. Ostrowska, S.; Maśliński, W.; Prochorec-Sobieszek, M.; Nieciecki, M.; Sudoł-Szopińska, I. Cartilage and bone damage in rheumatoid arthritis. *Reumatologia* **2018**, *56*, 111-120, <https://doi.org/10.5114/reum.2018.75523>.

Publisher's Note & Disclaimer

The statements, opinions, and data presented in this publication are solely those of the individual author(s) and contributor(s) and do not necessarily reflect the views of the publisher and/or the editor(s). The publisher and/or the editor(s) disclaim any responsibility for the accuracy, completeness, or reliability of the content. Neither the publisher nor the editor(s) assume any legal liability for any errors, omissions, or consequences arising from the use of the information presented in this publication. Furthermore, the publisher and/or the editor(s) disclaim any liability for any injury, damage, or loss to persons or property that may result from the use of any ideas, methods, instructions, or products mentioned in the content. Readers are encouraged to independently verify any information before relying on it, and the publisher assumes no responsibility for any consequences arising from the use of materials contained in this publication.

Supplementary Data

Table S1. Shows Stability studies data of prepared RTCPs (F3, F4) and RTNCPs (F1, F2) formulations.

Time (d)	Formulation code	Normal conditions (25± 2°C)				Refrigerated conditions (4± 2°C)			
		PS	PDI	DEE (%)	DL (%)	PS	PDI	DEE (%)	DL (%)
0	F1	335.6	0.269	71±2.13	1.97±0.12	335.6	0.269	71±2.13	1.97±0.12
	F2	429.5	0.252	67±3.10	1.94±0.09	429.5	0.252	67±3.10	1.94±0.09
	F3	527.6	0.348	81±2.09	2.30±0.21	527.6	0.348	81±2.09	2.30±0.21
	F4	548.4	0.324	77±2.50	2.13±0.13	548.4	0.324	77±2.50	2.13±0.13
30	F1	339.9	0.272	69±4.10	1.86±0.32	337.5	0.271	70±3.12	1.95±0.08
	F2	438.8	0.269	65±2.32	1.75±0.27	427.9	0.258	68±2.23	1.89±0.07
	F3	537.5	0.341	79±1.97	2.07±0.10	531.2	0.330	80±3.01	2.15±0.11
	F4	551.1	0.340	72±2.78	1.99±0.31	547.7	0.322	76±2.23	2.12±0.14
60	F1	357.1	0.280	67±2.33	1.70±0.12	348.9	0.276	70±2.29	1.83±0.08
	F2	455.7	0.290	60±3.11	1.67±0.18	439.1	0.285	65±3.14	1.80±0.11
	F3	549.2	0.350	75±3.23	1.92±0.13	536.9	0.335	78±3.19	2.19±0.12
	F4	562.4	0.352	66±1.98	1.87±0.10	557.1	0.336	74±3.14	2.10±0.18
90	F1	373.4	0.278	60±2.56	1.65±0.16	359.5	0.275	65±3.34	1.74±0.14
	F2	459.7	0.297	55±3.11	1.59±0.14	448.9	0.288	60±2.92	1.77±0.19
	F3	564.6	0.368	68±3.23	1.85±0.19	545.8	0.343	74±4.11	1.99±0.10
	F4	578.5	0.377	60±3.56	1.78±0.12	563.4	0.345	70±3.67	1.93±0.09

Table S2. Skin permeation parameters of different formulations. All data are presented as mean± SD (n=3).

Formulation	Q (µg/cm ²)	J _{ss} (mg/cm ² /h)	P _{app} (cm/h)
MGH1	218.97± 24.14	0.0620±0.01	0.086±0.02
MGH2	409.35± 35.68	0.2872±0.01	0.062±0.09
MGH3	604.33±23.16	0.4010±0.03	0.013±0.01

Where **Q** is the cumulative amount of drug permeated per unit area (µg/cm²) after 24 hours, **J_{ss}** is the permeation rate constant at steady state (µg/cm²/h), obtained from the slope of the regression line after plotting the cumulative amount of RT permeated per unit area vs. time. **P_{app}** is the apparent permeability coefficient (cm/h).

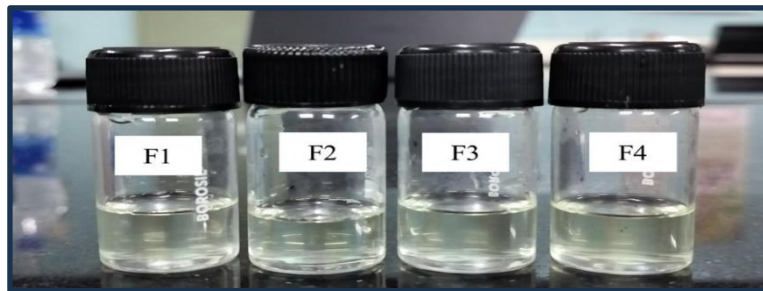


Figure S1. RTCPs (F3, F4) and RTNCPs (F1, F2) formulations were dispersed in distilled water.

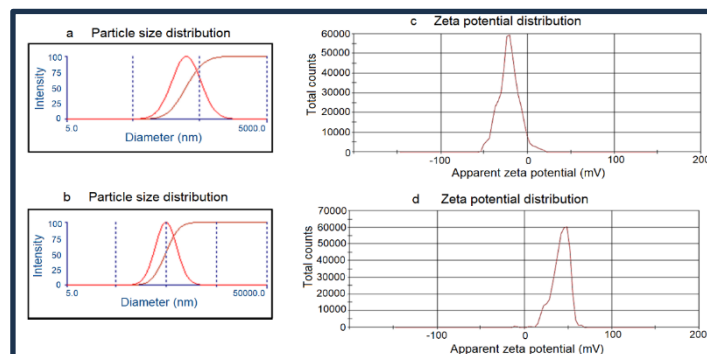


Figure S2. Particle size distribution of (a) RTNCPs (F2), (b) RTCPs (F3), and zeta potential distribution of (c) RTNCPs (F2), (d) RTCPs (F3).